ELSEVIER

Materials Science and Engineering A271 (1999) 449–457

MATERIALS SCIENCE & ENGINEERING A

www.elsevier.com/locate/msea

Cyclic deformation features of a copper bicrystal with an embedded grain and surrounding grain boundary

Z.F. Zhang *, Z.G. Wang

State Key Laboratory for Fatigue and Fracture of Materials, Institute of Metal Research, Chinese Academy of Sciences, 72 Wenhua Road, Shenyang 110015, People's Republic of China

Received 22 February 1999; received in revised form 8 June 1999

Abstract

Cyclic stress–strain response, surface slip morphology and saturation dislocation patterns in a copper bicrystal with an embedded grain G_E and a surrounding grain boundary (GB) were investigated and compared with those of its matrix monocrystal by multi-step cyclic straining at room temperature in air. The experimental results showed that the cyclic stress–strain (CSS) curve of the matrix monocrystal exhibited a plateau region with the saturation resolved shear stresses of 28.8–29.4 MPa in the plastic resolved shear strain range of 4.7×10^{-4}–3.18×10^{-3}. However, the copper bicrystal displayed relatively higher saturation stresses of 32.2–36.0 MPa, if modified by the orientation factor of the matrix grain, indicating no apparent plateau region in its CSS curve. Surface observations revealed that the primary slip system was dominant in both grains G_M and G_E except near the surrounding GB. By the electron channeling contrast (ECC) technique in scanning electron microscopy (SEM), the dislocation patterns of the bicrystal and the matrix monocrystal were observed. It was found that the two-phase structure of persistent slip bands (PSBs) and dislocation veins can nucleate in both grains G_M and G_E after cyclic deformation of the bicrystal. Based on the experimental results above, the effects of the surrounding GB and the embedded grain G_E on the cyclic stress–strain response of the bicrystal were discussed. Those results might provide an experimental evidence for understanding the difference in CSS curves between copper single- and poly-crystals.

Keywords: Copper bicrystal; Embedded grain; Grain boundary (GB); Cyclic stress–strain (CSS) curve; Slip morphology; Dislocation pattern

1. Introduction

As pointed out by Lukas and Kunz [1], the effects of grain boundaries (GBs) and component grains on the cyclic stress–strain response of polycrystals had not been clearly understood. It is well-known that the cyclic stress–strain (CSS) curve of the single-slip-oriented copper single crystal clearly shows three stages, i.e. A, B and C regions [2]. In particular, the saturation resolved shear stress nearly maintains the constant value of 28–30 MPa, which is independent of strain amplitude and crystal orientation in the region B of the CSS curve [3]. This saturation resolved shear stress is equal to the stress activating persistent slip bands (PSBs) [3,4]. Meanwhile, the CSS curves of polycrystalline copper have been widely investigated and the results showed a great difference with that of the copper single crystals [5–11]. Mughrabi [7], Lukas and Kunz [8] suggested that the plateau behavior in copper single crystals was associated with the formation of PSBs and no apparent plateau existed in the CSS curve of polycrystals. In particular, the effects of dislocation arrangements and GBs on the CSS response of polycrystals are not very clear. Bicrystals are often regarded as ideal model materials to reveal the effects of GBs and crystal orientations on the plastic deformation mechanisms [12–18]. It has been known that the flow stress of polycrystal is greater than that of a single crystal and multiple slip often occurs at the early stage of plastic deformation in polycrystal due to the presence of GBs [13–18]. However, the studies on the cyclic deformation behavior of bicrystals were rather scarce. In this series of work [19–24], the cyclic deformation behavior of copper bicrystals with perpendicular or parallel GB has been investigated systematically. It was found that the com-

* Corresponding author. Tel.: +86-24-2384-3531-55225.
E-mail address: zhfzhang@imr.ac.cn (Z.F. Zhang)

0921-5093/99/$ - see front matter
PII: S0921-5093(99)00312-3

ponent crystal orientations in a copper bicrystal with a perpendicular GB have a decisive effect on their CSS curves [19–22], however, a different degree of GB strengthening effect on the copper bicrystals with a parallel GB was observed [23,24]. In this paper, the cyclic deformation features of a copper bicrystal with an embedded grain G_E and a surrounding GB will be further investigated for better understanding the fatigue mechanism of polycrystals.

2. Experimental procedure

A copper bicrystal, in which a large grain G_E inlaid a matrix grain G_M, was grown from the OFHC copper of 99.999% purity by the Bridgman method in a horizontal furnace. Two fatigue specimens were prepared from the as-grown crystal. Fig. 1(a) is a fatigue specimen of the copper bicrystal (denoted as B) with an embedded grain G_E and a surrounding GB. Fig. 1(b) is a fatigue specimen of the matrix monocrystal (denoted as M). The specimen size and the orientation of the bicrystal and its matrix monocrystal are the same. By X-ray Laue back-reflection method, the stress axis orientation of the matrix monocrystal was determined as [$\bar{2}$57], a typical single-slip orientation. Whereas, the orientation of the embedded grain G_E was not examined because it is relatively small and difficult to be detected by this technique. Before cyclic deformation, both the bicrystal and the matrix monocrystal specimens were electro-polished carefully for surface observation. Symmetrical push–pull tests were performed on a Shimadzu servo-hydraulic testing machine under constant plastic strain control at room temperature in air. A triangle wave with a frequency range of 0.05–0.3 Hz was used. The peak loads in tension and compression were recorded continuously and the hysteresis loops were registered in interval on an X–Y recorder. The CSS curves of the bicrystal and the matrix monocrystal were determined by multi-step testing method. The applied axial plastic strain amplitude were 2.2×10^{-4}, 5.4×10^{-4}, 1.0×10^{-3} and 1.5×10^{-3}, respectively. After cyclic deformation under four-step strain amplitudes, the surface slip morphology was observed by optical microscopy (OM) and scanning electron microscopy (SEM), respectively.

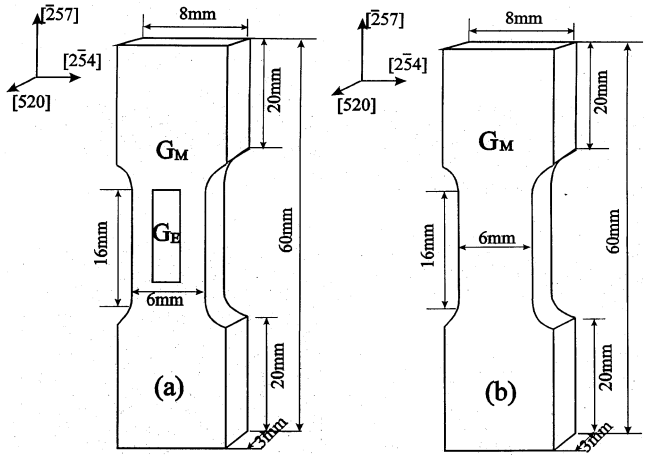

Fig. 1. Fatigue specimens of the copper bicrystal and the matrix monocrystal. (a) Copper bicrystal; (b) matrix copper monocrystal.

To examine the saturation dislocation patterns of the specimens, transmission electron microscopy (TEM) is a widely used method. However, TEM investigations require thin foil specimens and only a relatively small area can be investigated. Therefore, there are some disadvantages of the TEM technique which limit the field of applications. Recently, the electron channelling contrast (ECC) technique in SEM has been successfully applied to study the dislocation patterns in deformed metals [25,26], such as stainless steel [27], nickel [28,29], copper [30–32] and aluminum [33]. It has been generally recognized that the SEM-ECC technique can reveal some information which is difficult to achieve by conventional the TEM technique. For example, it allows the observations of dislocation patterns over the whole cross-section of the specimen, and especially at some special sites, such as in the vicinity of GB [22,34,35] and within deformation bands [30,31]. Therefore, the SEM-ECC technique was also used for the present study. The fatigued specimens were polished again to observe the surface dislocation patterns within grain and near the GB by the SEM-ECC technique. The operation conditions of the SEM-ECC technique can refer to the previous work [22,30–32,34,35]. In the end, the bicrystal specimen was cut from the middle part along the stress axis to observe the dislocation arrangements in the interior of the embedded grain G_E.

3. Experimental results

3.1. Cyclic hardening and saturation behavior

Fig. 2 shows the cyclic hardening curves of the bicrystal (B) and the matrix monocrystal (M). It can be seen that the cyclic stresses of the bicrystal are basically equal to those of the matrix monocrystal below 100 cycles at the axial plastic strain amplitude of 2.2×10^{-4}. With further cyclic deformation, the bicrystal began to show a relatively higher stress than the matrix monocrystal until cyclic saturation occurred. The matrix monocrystal began to saturate about at 8000–10 000 cycles with an axial saturation stress of 61.2 MPa. However, the cyclic number of saturation was in the range of 12 000–14 000 and shows a relatively higher saturation stress of 68.4 MPa. After cyclic saturation of the specimens, a higher strain amplitude was applied. It can be seen that both the bicrystal and the

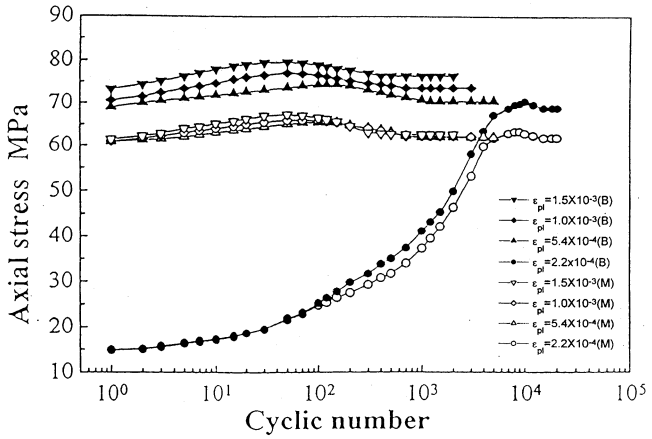

Fig. 2. Cyclic hardening curves of the copper bicrystal and the matrix monocrystal.

matrix monocrystal exhibited a small amount of initial hardening, consequent softening before saturated. The saturation stresses of the bicrystal and the matrix monocrystal at all the strain amplitudes are listed in Table 1. The CSS curves of the bicrystal and the matrix monocrystal are plotted in Fig. 3(a) and (b). It is apparent that the axial saturation stresses of the matrix monocrystal nearly maintains constant value of 61.2–62.1 MPa, i.e. its CSS curve shows an obvious plateau region at the applied strain range. By using the Schmid factor ($\Omega_M = 0.471$) of the [$\bar{2}$57] orientation, the plateau saturation resolved shear stress of the matrix monocrystal was calculated and is equal to 28.8–29.4 MPa. This result is in good agreement with that of the copper single crystal oriented for single-slip [2–4]. However, the saturation stress of the bicrystal is obviously higher than that of its matrix monocrystal and increases with strain amplitude, i.e. its CSS curve does not show a plateau behavior. If the saturation resolved shear stresses of the bicrystal were also calculated by using the Schmid factor of 0.471, they should be in the range of 32.2–36.0 MPa, which are apparently higher than those (28–30 MPa) of copper single crystal [2–4] or the matrix monocrystal. It is indicated that the embedded grain G_E and the surrounding GB should play certain

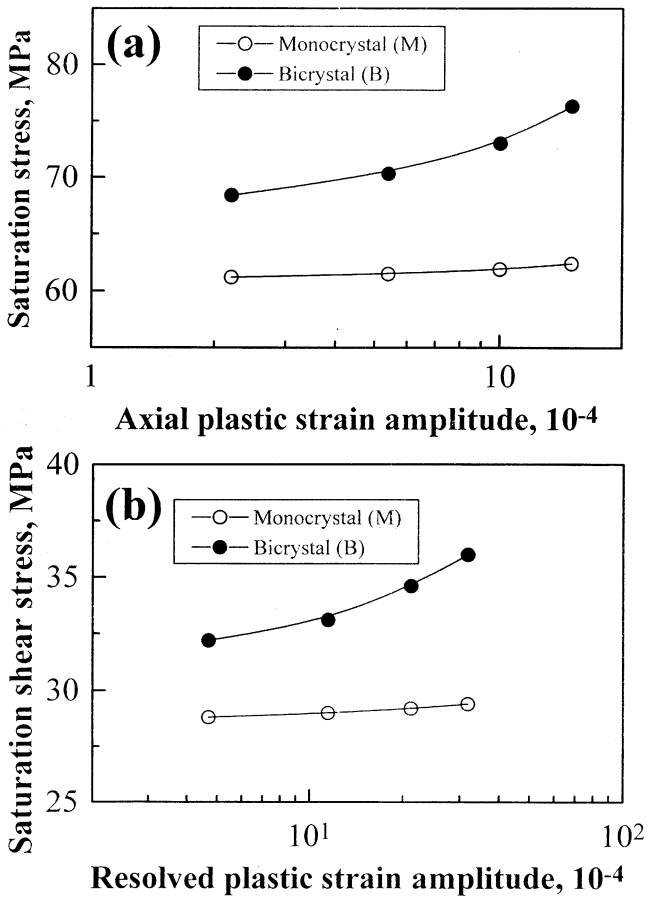

Fig. 3. Cyclic stress–strain curves of the copper bicrystal and the matrix monocrystal. (a) The curves of axial saturation stress vs axial plastic strain; (b) the curves of saturation resolved shear stress vs plastic resolved shear strain.

strengthening role in the bicrystal during cyclic deformation.

3.2. Slip morphology observation

Surface observations showed that only the primary slip system was activated in the matrix monocrystal at the applied strain range, which agrees well with its CSS curve (Fig. 3). However, the slip morphology of the

Table 1
Saturation stress and strain data of the bicrystal (B) and its matrix monocrystal (M)

Specimen	ε_{pl} ($\times 10^{-4}$)	σ_{as} (MPa)	γ_{pl} ($\times 10^{-4}$)	τ_{as} (MPa)	N (cycles)
Bicrystal (B)	2.2	68.4	4.7	32.2	20 000
	5.4	70.6	11.5	33.3	5000
	10	73.2	21.2	34.5	3000
	15	76.3	31.8	36.0	2000
Monocrystal (M)	2.2	61.2	4.7	28.8	20 000
	5.4	61.6	11.5	29.0	5000
	10	61.9	21.2	29.2	3000
	15	62.1	31.8	29.4	2000

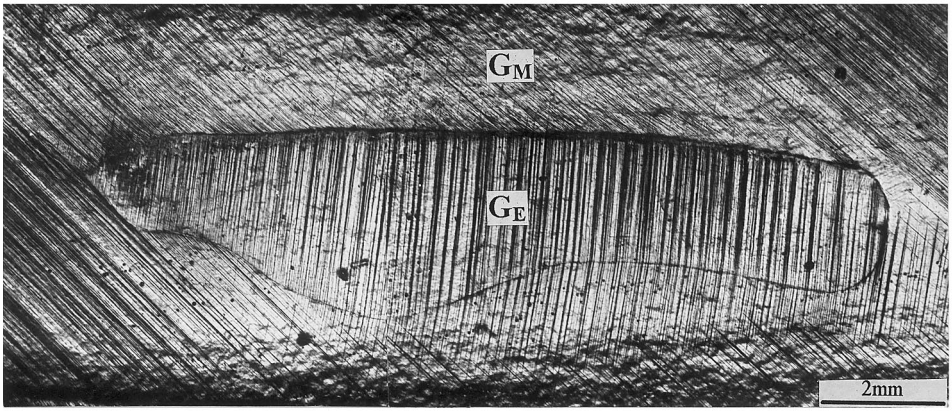

Fig. 4. Whole slip morphology of the bicrystal.

bicrystal exhibited different features. Fig. 4 shows the whole slip morphology of the cyclically saturated bicrystal by the four-step straining. The primary slip bands spread all over the area of the matrix grain G_M, but secondary slip lines were seen only near the surrounding GB. More detailed features of the slip bands within the grain G_M at one end of the embedded grain G_E were shown in Fig. 5(a). It is indicated that the embedded grain G_E became a strong obstacle to the primary slip bands within the matrix grain G_M during cyclic deformation. The secondary slip lines along surrounding GB were enlarged and shown in Fig. 5(b). It can be seen that the total number of the activated slip systems is basically equal to 4, which is in roughly consistent with the predication by Kocks [12]. Apparently, the surrounding GB can lead to the plastic strain incompatibility and the operation of secondary slip during cyclic deformation of the bicrystal. This result is well consistent with those observed in the fatigued copper bicrystals with a parallel GB [23,24]. In addition, there is only one group of primary slip bands within the embedded grain G_E except near the GB, as shown in Fig. 5(b). In particular, the primary slip bands within the embedded grain G_E are very coarse and can produce some affected zones within the grain G_M, indicating that strong plastic strain incompatibility and higher stress concentration near the GB may exist.

3.3. Observations on dislocation patterns by SEM-ECC technique

Instead of the commonly used TEM technique, the SEM-ECC technique was adopted for observing the dislocation patterns in the present study. The results show that the saturation dislocation patterns in the matrix monocrystal consisted of the two-phase structure [36], i.e. PSBs and dislocation veins, as shown in Fig. 6(a). This dislocation pattern is consistent with the plateau behavior in its CSS curve [36–38]. However, the dislocation patterns in the copper bicrystal displayed a different feature at different regions on its surface. Within the grain G_M, the dislocation patterns are also composed of the two-phase structure of PSBs and veins, similar to that in the matrix monocrystal. Fig. 6(b) and (c) show the dislocation patterns near the surrounding GB, it can be seen that the PSBs in both grains G_M and G_E can reach the GB, but can not

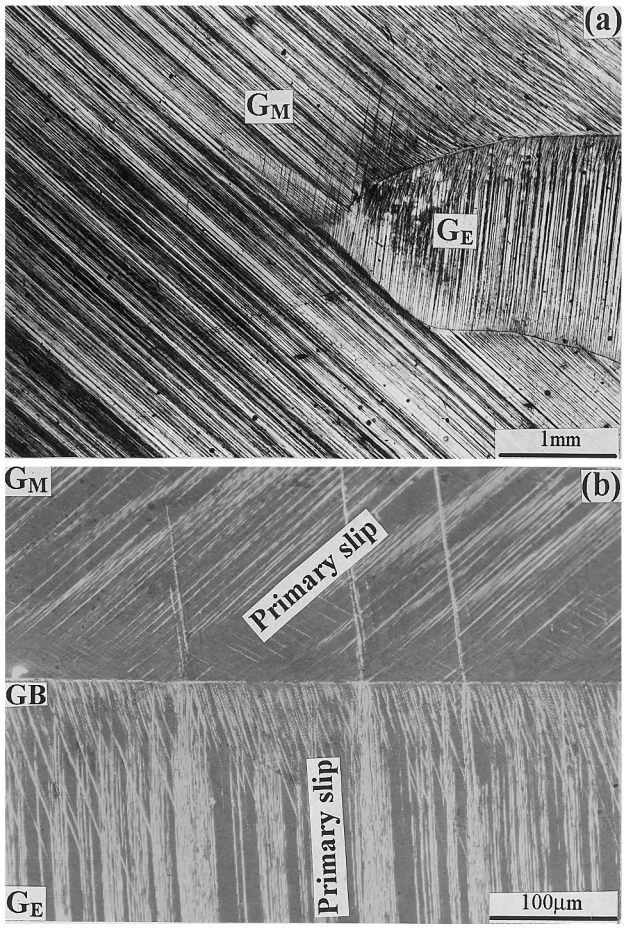

Fig. 5. Slip morphology near the GBs. (a) Slip morphology at one end of the embedded grain; (b) beside the surrounding GB.

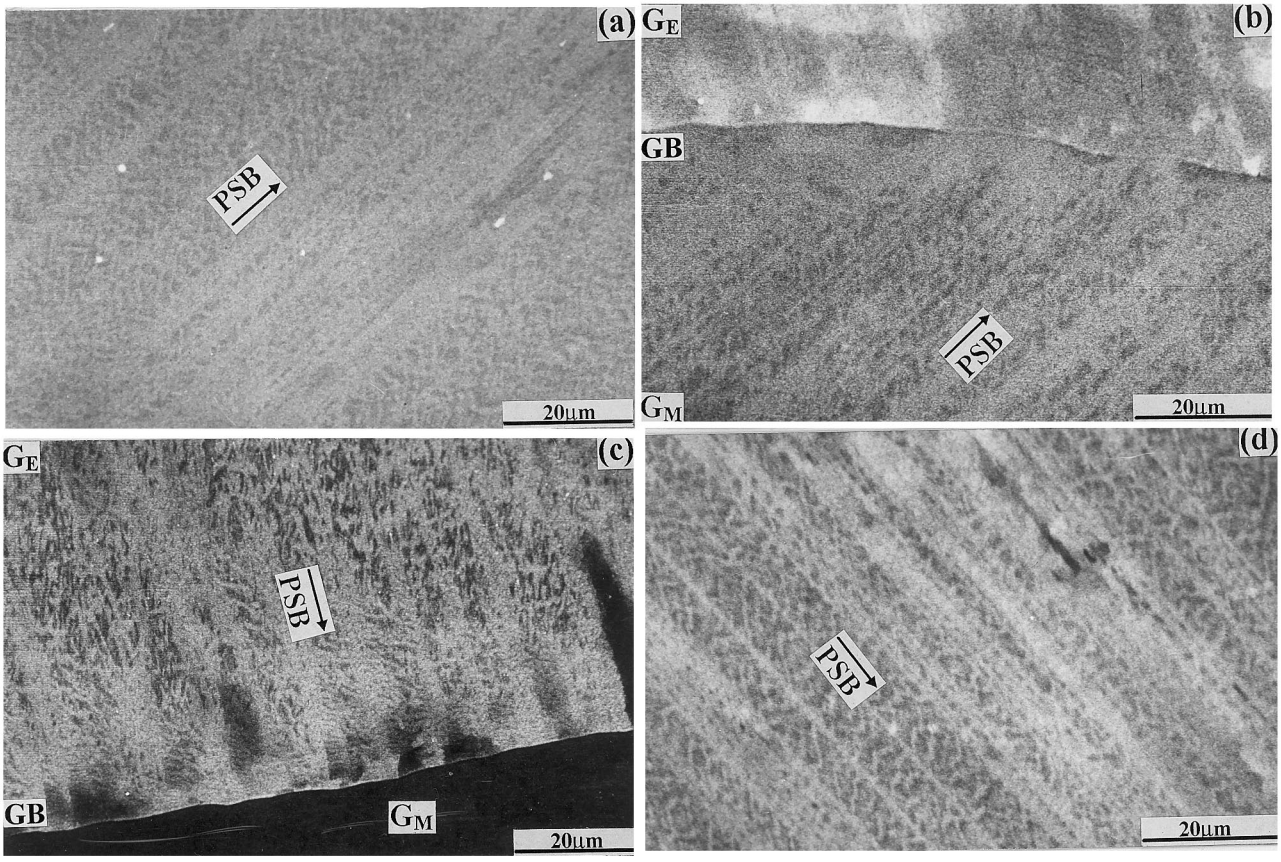

Fig. 6. Saturation dislocation patterns observed by the scanning electron microscopy (SEM)-electron channeling contrast (ECC) technique. (a) Dislocation pattern in the matrix monocrystal; (b) and (c) dislocation patterns near the surrounding grain boundary (GB); (d) dislocation patterns in the interior of the embedded grain.

transfer through it and became irregular and discontinuous. It is consistent with the surface slip morphology near the GB (in Fig. 5(b)). Those irregular dislocation should be the result of the operation of secondary slip near the GB. To further reveal the dislocation arrangements in the interior of the embedded grain, the bicrystal was cut from the middle part along the stress axis. The observations show that the embedded grain is approximately 1.5 mm in depth and the ladder-like PSB structure (Fig. 6(d)) is more striking than that on the surface. Clearly, the two-phase structure of PSBs and dislocation veins can nucleate in both grains G_M and G_E, but the ladder-like PSBs can not pass through the surrounding GB during cyclic deformation.

4. Discussion

4.1. Stress distribution analysis of the bicrystal

Based on the CSS curves (Fig. 3(a) and (b)) of the bicrystal and its matrix monocrystal, it can be assumed that their stress distributions may be shown in Fig. 7(a) and (b). As the matrix monocrystal was cyclically saturated, the plastic strains will be carried by the PSBs, as shown in Fig. 6(a) and illustrated in Fig. 7(a). It is well known that the plateau saturation resolved shear stresses of the single-slip-oriented copper single crystal at room temperature are in the range of 28–30 MPa, which correspond to the stress τ_{as}^{PSB} activating the PSBs. From Fig. 3(b), it is apparent that the saturation resolved shear stresses of the matrix monocrystal are in the range of 28.8–29.4 MPa, which are in good consistence with that in copper single crystals [2–4]. Consequently, as shown in Fig. 7(a), it can be considered that the saturation resolved shear stress τ_{as}^{M} of the matrix monocrystal should be equal to the stress τ_{as}^{PSB} activating PSBs, i.e.

$$\tau_{as}^{M} = \tau_{as}^{PSB} = \sigma_{as}^{M}\Omega_{M} \quad (1)$$

where, σ_{as}^{M} is the axial saturation stress, Ω_M is the Schmid factor of primary slip system of the matrix monocrystal and equal to 0.471. Similarly, as shown in Fig. 7(b), the saturation resolved shear stress τ_{as}^{B} of the bicrystal along the primary slip of the matrix grain G_M can be calculated as follows

$$\tau_{as}^{B} = \sigma_{as}^{B}\Omega_{M} \quad (2)$$

where, σ_{as}^{B} is the axial saturation stress of the bicrystal. SEM-ECC observations showed that the PSBs can also form within the embedded grain G_E, as shown in Fig. 6(b) and (c). Hence, it may be considered that the resolved shear stress τ_{as}^{E} along the primary slip of the embedded grain G_E can be calculated as

$$\tau_{as}^{E} = \tau_{as}^{PSB} = \sigma_{as}^{E}\Omega_E \quad (3)$$

where, σ_{as}^{E} is the axial saturation stress acting on the embedded grain G_E, Ω_E is the Schmid factor of activated slip system of the embedded grain. The calculated results by using Eqs. (1) and (2) are listed in Table 1. Apparently, the saturation stresses of the bicrystal are higher than those of the matrix monocrystal, the difference is

$$\Delta\tau_{as} = \tau_{as}^{B} - \tau_{as}^{M} = (\sigma_{as}^{B} - \sigma_{as}^{M})\Omega_M \quad (4)$$

It means that the surrounding GB and the embedded grain G_E should play a strengthening role in the bicrystal. The surface observations of slip bands and dislocation patterns might provide a powerful evidence for it. To better understand the effects of the embedded grain and the GB on the bicrystal, one can classify the stresses acting on the bicrystal into three parts, i.e. (1) axial saturation stress σ_{as}^{M} on the matrix grain G_M; (2) axial saturation stress σ_{as}^{E} on the embedded grain G_E; and (3) additional stress σ_{as}^{GB} caused by the surrounding GB. Those stresses should have the following relation

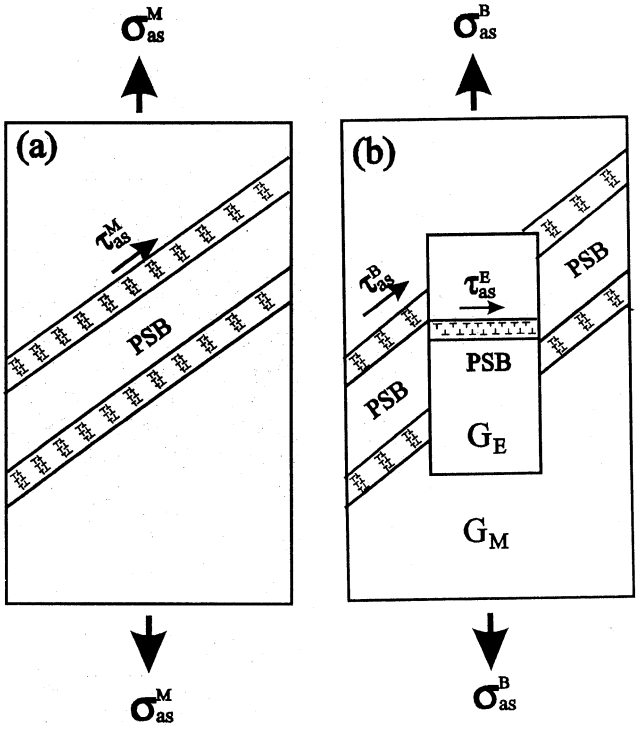

Fig. 7. Diagrammatic sketches of stress distribution in the bicrystal and the matrix monocrystal. (a) Stress distribution in the bicrystal; (b) stress distribution in the matrix monocrystal.

$$\sigma_{as}^{B} = \sigma_{as}^{M}V_M + \sigma_{as}^{E}V_E + \sigma_{as}^{GB} = \sigma_{as}^{M} + \sigma_{as}^{GB} + (\sigma_{as}^{E} - \sigma_{as}^{M})V_E \quad (5)$$

where, V_M and V_E are the volume fractions of the grains G_M and G_E in the bicrystal and $V_M + V_E = 1$. Rearranging Eq. (5) gives

$$(\sigma_{as}^{B} - \sigma_{as}^{M}) = \sigma_{as}^{GB} + (\sigma_{as}^{E} - \sigma_{as}^{M})V_E \quad (6)$$

Substituting Eqs. (1)–(4) into Eq. (6) gives

$$\Delta\tau_{as} = (\sigma_{as}^{B} - \sigma_{as}^{M})\Omega_M = \sigma_{as}^{GB}\Omega_M + (\sigma_{as}^{E} - \sigma_{as}^{M})\Omega_M V_E = \sigma_{as}^{GB}\Omega_M + \tau_{as}^{PSB}\left(\frac{\Omega_M}{\Omega_E} - 1\right)V_E \quad (7)$$

Since $\Delta\tau_{as}$ results from the existence of GB and the embedded grain, the following may be assumed

$$\Delta\tau_{as} = \Delta\tau_{as}^{GB} + \Delta\tau_{as}^{E} \quad (8)$$

where,

$$\Delta\tau_{as}^{GB} = \sigma_{as}^{GB}\Omega_M \quad (9)$$

$$\Delta\tau_{as}^{E} = \tau_{as}^{PSB}\left(\frac{\Omega_M}{\Omega_E} - 1\right)V_E \quad (10)$$

$\Delta\tau_{as}^{GB}$ is strengthening stress caused by the GB, $\Delta\tau_{as}^{E}$ can be defined as strengthening or weakening stress caused by the embedded grain. Therefore, the stress difference $\Delta\tau_{as}$ between the bicrystal and its matrix monocrystal should be affected by $\Delta\tau_{as}^{GB}$ and $\Delta\tau_{as}^{E}$, or the GB and the embedded grain. The effects of the surrounding GB and the embedded grain will be discussed in the following sections, respectively.

4.2. Effect of the surrounding grain boundary

By observing the surface slip morphology of the bicrystal, it can be seen that the secondary slip lines were activated beside the GB, indicating that the serious plastic strain incompatibility occurred near the GB during cyclic deformation. For the bicrystals [13–18] subjected to plastic deformation, it has been proved that the plastic strain incompatibility often led to the operation of secondary slip and produced GB strengthening effect on the bicrystals. Recently, the strengthening mechanism of the GB on copper bicrystal under cyclic loading was discussed in detail [23,24]. It was found that the strengthening effect of GB on [$\bar{6}$79]/[$\bar{1}$45] copper bicrystal increased with strain amplitude and led to the disappearance of plateau region of its CSS curve. This GB strengthening effect was attributed to the GB resistance to the PSBs [24]. By the SEM-ECC technique, it has been observed that the ladder-like PSB structures became irregular and discontinuous near the GB (see Fig. 6(b) and (c)). Those observations should support a powerful evidence for the GB strengthening

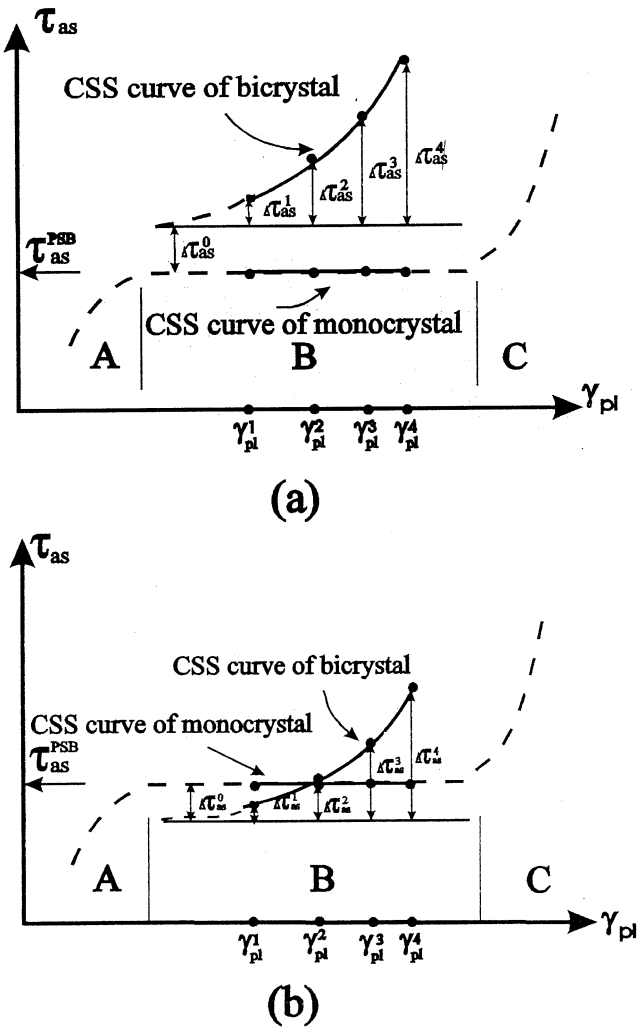

Fig. 8. Diagrammatic sketches of the cyclic stress–strain (CSS) curves between the bicrystal and the matrix monocrystal. (a) The Schmid factor Ω_M of the matrix grain is higher than that Ω_E of the embedded grain; (b) the Schmid factor Ω_M of the matrix grain is lower than that Ω_E of the embedded grain.

effect on the bicrystal. Based on the results above, it is possible that the surrounding GB will also play a remarkable strengthening effect on the bicrystal during cyclic deformation. The stress difference $\Delta\tau_{as}$ between the bicrystal and its matrix monocrystal can be partly attributed to the additional stress $\Delta\tau_{as}^{GB}$ caused by GB. Therefore, it can be concluded that the additional stress $\Delta\tau_{as}^{GB}$ of the GB to PSBs within the grains G_M and G_E may be increased with increasing plastic strain amplitude, as shown in Fig. 8(b). Meanwhile, $\Delta\tau_{as}^{GB}$ may be a function of plastic strain amplitude during cyclic deformation

$$\Delta\tau_{as}^{GB} = \Delta\tau_{as}^{i} = f(\gamma_{pl}^{i}) \tag{11}$$

If the Schmid factor ratio Ω_M/Ω_E of the grain G_M to grain G_E is considered, the relation of the CSS curves between the bicrystal and its matrix monocrystal can be classified into two cases, as shown in Fig. 8(a) and (b), and will be further discussed in the next section. At all the four strain amplitudes, the additional stress $\Delta\tau_{as}^{GB}$ to PSBs will not be a constant, but increased with strain amplitude, i.e.

$$\begin{aligned}
\Delta\tau_{as}^{GB}(\gamma_{pl}^{1}) &= \Delta\tau_{as}^{1}\\
\Delta\tau_{as}^{GB}(\gamma_{pl}^{2}) &= \Delta\tau_{as}^{2}\\
\Delta\tau_{as}^{GB}(\gamma_{pl}^{3}) &= \Delta\tau_{as}^{3}\\
\Delta\tau_{as}^{GB}(\gamma_{pl}^{4}) &= \Delta\tau_{as}^{4}
\end{aligned} \tag{12}$$

where, $\gamma_{pl}^{1} = 2.2\times10^{-4}/\Omega_M$, $\gamma_{pl}^{2} = 5.4\times10^{-4}/\Omega_M$, $\gamma_{pl}^{3} = 1.0\times10^{-3}/\Omega_M$, $\gamma_{pl}^{4} = 1.5\times10^{-3}/\Omega_M$, and

$$\Delta\tau_{as}^{1} < \Delta\tau_{as}^{2} < \Delta\tau_{as}^{3} < \Delta\tau_{as}^{4} \tag{13}$$

From Eqs. (12) and (13), it can be clearly understood why the saturation stresses of the bicrystal increased with strain amplitude and the plateau region of its CSS curve disappeared.

4.3. Effect of the embedded grain

By the observations of surface slip morphology and dislocation patterns, the two-phase structure of PSBs and dislocation veins can form in both grains G_M and G_E after cyclic deformation of the bicrystal. If the stress activating the PSBs within grains G_M and G_E is the same and ranges from 28 to 30 MPa, the effect of the embedded grain G_E on the bicrystal can be classified into two cases according to the Schmid factor ratio Ω_M/Ω_E of the grain G_M to grain G_E. (1) As the Schmid factor Ω_M of the grain G_M is higher than that Ω_E of the grain G_E, i.e. $\Omega_M/\Omega_E > 1$, the axial stress σ_{as}^{E} applying on the grain G_E will be higher than that σ_{as}^{M} acting on the matrix grain G_M during cyclic saturation. That means

$$\frac{\tau_{as}^{PSB}}{\Omega_M} = \sigma_{as}^{M} < \sigma_{as}^{E} = \frac{\tau_{as}^{PSB}}{\Omega_E} \tag{14}$$

From Eq. (10), one can know that

$$\frac{\Omega_M}{\Omega_E} > 1, \quad \Rightarrow \Delta\tau_{as}^{E} > 0 \tag{15}$$

Consequently, it can be concluded that the embedded grain should play a strengthening effect on the bicrystal since $\Delta\tau_{as}^{E}$ is a positive value. In this case, the relation of the CSS curves between the bicrystal and its matrix monocrystal will be illustrated in Fig. 8(a). The saturation resolved shear stress of the bicrystal at all the strain amplitudes will be always higher than that of the matrix monocrystal. The present bicrystal is very similar to the case in Fig. 8(a). On the contrary, as the Schmid factor Ω_M of the grain G_M is lower than that Ω_E of the grain G_E, i.e. $\Omega_M/\Omega_E < 1$, the axial stress σ_{as}^{E} applying on the grain G_E will be lower than that σ_{as}^{M}

acting on the grain G_M during cyclic saturation. That means

$$\frac{\tau_{as}^{PSB}}{\Omega_M} = \sigma_{as}^{M} > \sigma_{as}^{B} = \frac{\tau_{as}^{PSB}}{\Omega_E} \quad (16)$$

Similarly, from Eq. (10), it has the following relation

$$\frac{\Omega_M}{\Omega_E} < 1, \quad \Rightarrow \Delta\tau_{as}^{E} < 0 \quad (17)$$

Under this condition, it can be considered that the grain G_E should play a weakening effect on the bicrystal because $\Delta\tau_{as}^{E}$ is a negative value. As a result, the relation of the CSS curves between the bicrystal and its matrix monocrystal will be illustrated in Fig. 8(b). At low strain amplitude, the saturation stress τ_{as}^{B} of the bicrystal may be lower than that τ_{as}^{M} of the monocrystal. With increasing strain amplitude, the saturation stress τ_{as}^{B} of the bicrystal will be increased owing to the GB strengthening effect $\Delta\tau_{as}^{GB}$, however, the saturation stress τ_{as}^{M} of the monocrystal still maintains the constant value. At intermediate strain amplitude, the saturation stress τ_{as}^{B} of the bicrystal may be equal to that τ_{as}^{M} of the monocrystal, indicating that the strengthening effect $\Delta\tau_{as}^{GB}$ caused by the GB is equal to the weakening effect $\Delta\tau_{as}^{E}$ by the embedded grain. Obviously, the present results of the bicrystal can be illustrated in Fig. 8(a), which is different from the case in Fig. 8(b). From Eq. (10), if the volume faction V_E and the Schmid factor Ω_E of the embedded grain are constant, the strengthening or weakening effect $\Delta\tau_{as}^{E}$ caused by the embedded grain should also be constant, i.e.

$$\Delta\tau_{as}^{E} = \tau_{as}^{PSB}\left(\frac{\Omega_M}{\Omega_E} - 1\right)V_E = \text{Constant} \quad (18)$$

For the present bicrystal, the Schmid factor Ω_M of the grain G_M is equal to 0.471, nearly reaches the maximum value of 0.5, however, the orientation of the embedded grain is unknown. By analogy with correlation of their CSS curves, it is suggested that the effect of the embedded grain should belong to the case in Fig. 8(a).

5. Conclusions

By comparing the cyclic deformation behavior of a copper bicrystal containing an embedded grain with that of its matrix monocrystal, the following conclusions can be drawn.

(1) The bicrystal exhibited obviously higher stress than its matrix monocrystal during cyclic deformation. The CSS curve of the monocrystal showed a plateau region with the saturation stress τ_{as}^{M} of 28.8–29.4 MPa, however, the saturation stress τ_{as}^{B} of the bicrystal was increased from 32.2 to 36.0 MPa and there was no any plateau region in its CSS curve.

(2) Surface observations showed that the slip bands were discontinuous in the bicrystal and the secondary slip bands were activated beside the surrounding GB. By SEM-ECC technique, it is found that the two-phase structure of ladder-like PSBs and dislocation veins can form in both grains G_M and G_E, as well as in the matrix monocrystal. The PSBs became irregular and discontinuous as they reached the GB. In particular, PSBs can nucleate in the interior of the embedded grain.

(3) By analyzing the stress distributions in the bicrystal and its matrix monocrystal, It is indicated that the surrounding GB should always play a strengthening effect on the bicrystal and lead to the disappearance of plateau region of its CSS curve. The embedded grain should provide a strengthening effect on the present bicrystal. Those results might provide an experimental evidence for the controversy about the CSS curves between copper single- and poly-crystals.

Acknowledgements

This work was financially supported by the National Nature Science Foundation of China (NSFC) under grant numbers 19392300-4 and 59701006. The authors are grateful for those supports. In addition, the authors would like to express their appreciation to Professor Z.R. Wang at the University of Toronto, Canada for his helpful comments and suggestions.

References

[1] P. Lukas, L. Kunz, Mater. Sci. Eng. 189A (1994) 1–7.
[2] H. Mughrabi, Mater. Sci. Eng. 33 (1978) 207–223.
[3] A.S. Cheng, C. Laird, Mater. Sci. Eng. 51 (1981) 111–121.
[4] Z.S. Basinski, S.J. Basinski, Prog. Mater. Sci. 36 (1992) 89–148.
[5] K.V. Rasmussen, O.B. Pedersen, Acta Metall. 28 (1980) 1467–1478.
[6] S.P. Bhat, C. Laird, Scripta Metall. 12 (1978) 687–692.
[7] H. Mughrabi, Scripta Metall. 13 (1979) 479–484.
[8] P. Lukas, L. Kunz, Mater. Sci. Eng. 85 (1987) 67–75.
[9] A.T. Winter, Acta Metall. 28 (1980) 693–694.
[10] O.B. Pedersen, K.V. Rasmussen, A.T. Winter, Acta Metall. 30 (1982) 57–62.
[11] C.D. Liu, M.N. Bassim, D.X. You, Acta Metall. Mater. 42 (1994) 3695–3704.
[12] U.F. Kocks, Philos. Mag. 10 (1964) 187–192.
[13] S. Miura, Y. Saeki, Acta Metall. 26 (1978) 93–101.
[14] S. Miura, K. Hamashima, K.T. Aust, Acta Metall. 28 (1980) 1591–1602.
[15] C. Rey, A. Zaoui, Acta Metall. 28 (1980) 687–697.
[16] C. Rey, A. Zaoui, Acta Metall. 30 (1982) 523–535.
[17] Y.-D. Chuang, H. Margolin, Metall. Trans. 4A (1973) 1905–1917.
[18] J.P. Hirth, Metall. Trans. 3A (1972) 3047–3067.
[19] Y.M. Hu, Z.G. Wang, Int. J. Fatigue 19 (1997) 59–65.
[20] Y.M. Hu, Z.G. Wang, Acta Mater. 45 (1997) 2655–2670.
[21] Z.F. Zhang, Z.G. Wang, Mater. Sci. Eng. 255A (1998) 148–153.
[22] Z.F. Zhang, Z.G. Wang, Philos. Mag. Lett. 78 (1998) 105–113.

[23] Y.M. Hu, Z.G. Wang, G.Y. Li, Mater. Sci. Eng. 208A (1996) 260–269.
[24] Z.F. Zhang, Z.G. Wang, Metall. Mater. Trans. 29A (1998) 2563–2569.
[25] A.J. Wilkinson, P.B. Hirsch, Philos. Mag. 74 (1995) 81–103.
[26] A.J. Wilkinson, M.B. Henderson, J.W. Martin, Philos. Mag. Lett. 74 (1996) 145–151.
[27] R. Zauter, F. Petry, M. Bayerlei, C. Sommer, H.-J. Christ, H. Mughrabi, Philos. Mag. 66 (1992) 425–436.
[28] A. Schwab, J. Bretschneider, C. Buque, C. Blochwitz, C. Holste, Philos. Mag. Lett. 74 (1996) 449–454.
[29] J. Bretschneider, C. Holste, B. Tippelt, Acta Mater. 45 (1997) 3755–3783.
[30] B. Gong, Z.R. Wang, D.L. Chen, Z.G. Wang, Scripta Mater. 37 (1997) 1605–1610.
[31] X.W. Li, Y.M. Hu, Z.G. Wang, Mater. Sci. Eng. A248 (1998) 299–303.
[32] D. Melisova, B. Weiss, R. Stickler, Scripta Mater. 36 (1997) 1061–1066.
[33] D.R.G. Mitchell, R.A. Day, Scripta Mater. 39 (1998) 923–930.
[34] Z.F. Zhang, Z.G. Wang, Acta Mater. 46 (1998) 5063–5072.
[35] Z.F. Zhang, Z.G. Wang, Philos. Mag. 79A (1999) 741–752.
[36] A.T. Winter, Philos. Mag. 30A (1974) 719–738.
[37] J.M. Finney, C. Laird, Philos. Mag. 31A (1975) 339–366.
[38] C. Laird, P. Charsley, H. Mughrabi, Mater. Sci. Eng. 81 (1986) 433–450.